Development of Mg^{2+} ion-selective microelectrodes for potentiometric Scanning Electrochemical Microscopy monitoring of galvanic corrosion processes

Javier Izquierdo[a], András Kiss[b], Juan José Santana[a,c], Lívia Nagy[b], István Bitter[d], Hugh S. Isaacs[e], Géza Nagy[b], Ricardo M. Souto[a,f]

[a] *Department of Physical Chemistry, University of La Laguna, E-38200 La Laguna, Tenerife, Canary Islands, Spain*
[b] *Department of General and Physical Chemistry, Faculty of Sciences, University of Pécs, 7624 Pécs, Ifjúság útja 6, Hungary*
[c] *Department of Process Engineering, University of Las Palmas de Gran Canaria, E-35017 Las Palmas de Gran Canaria, Canary Islands, Spain*
[d] *Budapest University of Technology and Economics, Budafoki u. 8, 1111 Budapest, Hungary*
[e] *Chemistry Department, Brookhaven National Laboratory, Upton, NY 11973, USA*
[f] *Instituto Universitario de Materiales y Nanotecnologías, University of La Laguna, E-38200 La Laguna, Tenerife, Canary Islands, Spain*

Abstract

The fabrication of a solid-contact, micropipette-based magnesium ion-selective micro-tipped electrode (ISME) suitable for scanning electrochemical microscopy is reported.and compared against a conventional micro-tipped ISME having a conventional aqueous internal reference electrode. Measurements showed that the solid-contact ISME had a lower internal resistance and a faster response time than the one with a liquid-contact These advantages increased the spatial distribution and improved 2D images depicting concentration distributions of Mg^{2+}. The ability of the microelectrode to image local ionic concentration has been tested over magnesium surfaces freely corroding or galvanically coupled to iron in aqueous chloride-containing solution. Scans of magnesium ion distribution, in the absence of corrosion currents, were also made over a micro-pipette source containing a concentrated magnesium chloride gel as a source pf Mg^{2+} and over a current source in the absence of Mg^{2+}. From these measurements it was concluded that the potentiometric measurements over corroding surfaces were dominated by the changes in Mg^{2+} distributions with small electric potential contributions due to corrosion current.

Keywords: scanning electrochemical microscopy; magnesium ion-selective electrode; potentiometric operation;; anodic dissolution; galvanic corrosion.

Introduction

Magnesium and its alloys have a major potential for use in many industrial sectors, particularly in automotive, aerospace and biomaterials industries, because of their high strength to weight ratio. Unfortunately, the resistance of magnesium and its alloys against corrosion in aqueous media is poor [1-4], thus requiring the development of improved corrosion-resistant alloys, inhibitor and protective coatings. Currently, understanding the characteristics of metal dissolution and passivity for these materials remains a major challenge, for conflicting ideas and results have been presented [5-10]. Oxide films formed on magnesium are less stable than the passive films formed on industrial metals and alloys owing to the low Pilling-Bedworth-ratio of $Mg(OH)_2$ [11], leading to pitting and general corrosion [12]. Indeed, Song and co-workers [13,14] suggested that corrosion of magnesium and its alloys is initiated from free-film region where the pitting corrosion is the main corrosion form. Additionally, these materials exhibit the behaviour that anodic polarization results in increased hydrogen production when they are exposed to chloride-containing electrolytes similar to what is observed during pitting of aluminum [15]. To account for this so-called "Negative Difference Effect" [3,16], it has been proposed that the poorly protective film developed on the surface of magnesium involves the formation of intermediate magnesium(I) species [6,17-20], which directly react with water leading to local alkalization and hydrogen gas evolution [19]. Though evidences for such a mechanism have been presented from the use of a variety of techniques [19,21,22], recent contributions claim that catalytic activation of the cathodic reaction can be induced by the anodic dissolution reaction [23-25], that is, Mg dissolves with a stoichiometry close to n = 2, and these reactions are highly localized.

Chemical imaging of reactive surfaces with high spatial resolution has become available with the introduction of scanning electrochemical microscopy (SECM). In fact, this technique has become a powerful tool in the study of a wide range of corrosion processes [26-28]. Despite the success of SECM in corrosion science, the investigation of dissolution processes in a number of technologically-relevant metals such as magnesium, aluminum and zinc, has not been monitored with the SECM using conventional amperometric microdisks due to their very negative redox potentials. The use of noble metal tips coated by metals that present wider stability potential ranges for water have allowed more negative potentials to be reached [29], still there are applications beyond those attained in this way. An alternate approach is the use of microsized ion-selective pipette electrodes as measuring tips because they provide the selectivity in chemical imaging [30], which is desirable to investigate the different stages of corrosion processes occurring in micrometric and submicrometric dimensions. As a result, scanning electrochemical microscopy will find an even wider application in materials science and corrosion technology. Unfortunately, ion-selective micropipette electrodes are rather fragile

tools, and operation lifetime of these probes is seldom longer than a few days. Mechanical contact or electrical shock easily can damage them. Furthermore, the electrical resistances of these “conventional” ion-selective micropipettes are high necessitating special electric shielding and a very slow scanning rate. This often hinders their applicability to corroding systems.

An improved ISME performance has been found with electrodes of specially prepared carbon fiber that could be placed close to the orifice of the micropipette. The internal contact potential remains constant by applying a doped, electrochemically-prepared conductive polymer coating on the carbon fiber surface based from 3,4-ethylenedioxythiophene (PEDOT) [31], thus accounting for reversibility. The life times of these new micropipettes were found surprisingly long; many performed well many monthsr after their preparation. Application include an ammonium and a xxx ISME [31 32]. More recently, we constructed a zinc(II) ion-selective microelectrode which for the first time allowed local zinc ion concentrations during the galvanic corrosion of a Fe/Zn couple to be imaged [33]. High spatial resolution was further developed employing a combined amperometric/potentiometric operation methodology for ISME [34] by using materials that exhibit a dual-function in different potential ranges as ultramicroelectrode (UME) tips [35,36]. This is the case with antimony as its open circuit potential responds to the pH of the environment [37].

Once the capability of these micropipette measuring tips in corrosion studies was demonstrated, our investigation focused on the fabrication of a Mg^{2+} ion-selective microelectrode. The first neutral carrier-based ion-selective electrodes for magnesium reported in the scientific literature were developed to monitor the hardness of water of different origins [38-40]. From those studies it was concluded that the best selectivity against sodium ion was achieved using amidic-based ionophores. Indeed, an amidic ionophore, octamethylenbis (N,N″-octamethylene-bis(N′-heptyl-N′-methyl-methylmalonamide) (ETH 5214), was used to build a liquid-contact magnesium ISME that was able to measure Mg^{2+} ion distributions over a Mg-based alloy in aqueous chloride-containing solution [41,42]. Another amidic ionophore, bis-N,N-dychlohexyl-malonamide [43], was employed for the fabrication of a Mg^{2+}-ion selective electrode tip for ISME for the first time [44]. In that work, a liquid-contact ion-selective micropipette electrode configuration was employed. Spatially-resolved data showing a major production of hydroxyl anions at the cathodic sites as result of oxygen reduction and local acidification in the vicinity of magnesium dissolution sites were obtained. Yet, the rather slow response times of the ion-selective microelectrode tips employed in the work severely limited the mapping capabilities of the technique and only selected one-dimensional line scans could be recorded at that time [44].

In this work, the fabrication and characterization of a new, faster, robust, solid-contact, micropipette-based magnesium ion-selective electrode suitable for use as an ISME is described. The electrodes were constructed using a carbon fiber coated by a conductive

polymer as internal contact. These electrodes had a higher resolution with lower resistance. Conventional micropipette Mg^{2+} selective electrodes were also fabricated for the sake of comparison. Our results on the galvanic corrosion of magnesium connected to iron in chloride solutions demonstrate that this Mg^{2+} ISME with carbon fiber internal electrodes can be employed for corrosion studies.

Experimental

Reagents and samples: Selectophore grade poly(vinyl chloride) (PVC), ortho-nitrophenyl octyl ether (o-NPOE), potassium tetrakis(4-chlorophenyl)-borate (PTCB), tetrahydrofurane (THF), and tris(hydroxymethyl)aminomethane (TRIS) were supplied by Fluka (Buchs, Switzerland). Carbon fiber of 33 μm diameter was provided by Specialty Materials (Lowell, MA, USA) as a generous gift. The carbon fibers were coated with a conductive polymer. Thus, 3,4-ethylenedioxythiophene (EDOT) (ref CH04M006) monomer obtained from Starck (Golar, Germany) was electropolymerized in 1-butyl-3-methyl-imidazoliumhexafluorophosphate ($BMIM^+$ PF_6^-) ionic liquid solvent from Solvent Innovation (Cologne, Germany). Analytical grade magnesium chloride hexahydrate Merck (Darmstadt, Germany). Chemicals were used as received. Aqueous solutions were prepared using ultra-pure deionized water.

A magnesium/iron galvanic couple was used as model corroding system. Iron wire 760 μm diameter and magnesium ribbon with 200 μm x 800 μm cross section were employed. The two metals were mounted in an *Epofix* resin disk (Struers, Ballerup, Denmark). Only their cross sections were exposed on the front side of the disk-shaped resin mounting (dia. 3 cm), and they extended about 15 mm at the rear of the mount for electric connection. The front side of the mounts was polished with silicon carbide paper down to 4000 grit. The surface was degreased with acetone, abundantly rinsed with ultra-pure deionized water and allowed to dry in air. When tested, the front side of the mount faced upwards surrounded laterally by a small section of PVC plastic tubing creating a small container holding 5 mL of 1 mM NaCl test electrolyte solution, **Figure 1A** and a 3M KCl Ag/AgCl reference electrode.

Detection of Mg^{2+} in a solution free of electric currents was conducted in a validation cell, **Figure 1B** of similar construction to **1A**. The cell held a small embedded glass micropipette with a diameter of 200 μm about 10 mm long. The micropipette was filled with 0.1 M $MgCl_2$ + 1mM NaCl contained in 4% agar-agar gel to establish a stable Mg^{2+} diffusion source and prevent the solution incursions when using only the $MgCl_2$ in a liquid aqueous solution.

The effect on the performance of the ion selective microelectrodes due to of electric fields with currents in the electrolyte was explored using two different arrangements electrodes

acting as point current source. Firstly, a noble metal disk microelectrode was considered. In this case, we employed two 100 μm diameter Pt-Ir wires. They were embedded in *Epofix* resin with only cross sections exposed to the electrolyte. One serving as current source was placed normal to the surface to offer a 100 μm diameter disk surface, whereas the other serving as counter electrode was placed with a certain tilt in order to offer a larger elliptical area. In the second arrangement, a glass micropipette with a tip diameter of 113 μm was employed as the current source and dipped into the electrolyte in a small container. A platinum electrode was inserted in the pipette. Another platinum wire was present in the electrolyte and acted as a counter electrode. Batteries and resistors were used to vary the current thorough the pipette which was measured with a ammeter.

Preparation of the ion-selective magnesium micropipette electrodes: The ionophore employed for the fabrication of the Mg^{2+} ISE was bis-N,N-dychlohexyl-malonamide, which was synthesized following the method described in reference [43]. Selectivity coefficients of this ionophore towards Na^+ and H^+ ions are also available there [43]. The composition of the ion-selective cocktail is given in **Table 1**. All the components in the ionophore cocktail were supplied by Sigma-Aldrich, except the home-made ionophore. Ion-selective microelectrodes were prepared using micropipettes pulled from borosilicate glass capillaries B100-50-10 (Sutter, Novato, CA, USA). The glass capillaries were first soaked in “piranha solution”, then thoroughly washed with twice deionized water and ethanol, and dried in oven at 105 ^{0}C. Micropipettes were pulled from the capillaries by using a pipette puller (Sutter Instruments, type P-30, Novato, CA, USA). The inner wall of the pipette tips were hydrophobized by exposing them to a solution of dimethyldichlorosilane in carbon tetrachloride through capillary action, and baking them at 200 ^{0}C for 30 minutes in a closed petri dish.

Figure 2 shows the sketches and micrographs of the liquid-contact and solid-contact ion-selective microelectrodes employed in this work, both using the same ion-selective cocktail but differing exclusively in the design of the electrochemical contact and the internal reference inside the micropipette electrode. The conventional micropipette Mg^{2+}-selective electrodes were prepared as described elsewhere [31]. The ionophore cocktail was filled into the micropipette tip under vacuum, whereas the internal solution was backfilled with the assistance of a microsyringe. The internal filling solution was 10 mM $MgCl_2$ + 0.25 M KCl, and the internal reference electrode was a chlorinated silver wire. The internal solution and the reference electrode were confined in the micropipette with *Loctite*® adhesive. Sketch and micrograph of the liquid-contact ion-selective microelectrode were shown in **Figure 2A**.

The solid-contact ion-selective microelectrodes were built using the same components employed for the fabrication of the conventional ISME, though in this case the internal contact was provided by a 33 μm diameter carbon fiber cut to 35 mm length. A copper wire was

previously attached to the carbon fiber using silver epoxy adhesive, to provide electric contact. The portion of the fiber to be contacting the ionophore cocktail was then coated with PEDOT conductive polymer in an electrochemical cell composed by the carbon fiber as working electrode, an Ag/AgCl wire immersed in the electrolyte as reference electrode, and a platinum wire as the auxiliary electrode. The monomer employed was 3,4-ethylenedioxythiophene dissolved in $BMIM^+$ PF_6^- ionic liquid [31]. Oxygen was purged from the EDOT-containing solution with nitrogen gas before and during the polymerization step. The resulting coated tip of the carbon fibre was immersed to a depth of 20 mm in the ionophore cocktail. The top of the micropipette electrode was sealed using Loctite® adhesive. A micrograph of the resulting microelectrode is depicted in **Figure 2B**.

A voltage divider method was employed to determine the resistance of the microelectrodes using 1 mM $MgCl_2$ + 1 mM NaCl solution. The electrochemical cell consisted of an Ag/AgCl, 3M KCl reference electrode and a freshly prepared microelectrodes. Their potentials were recorded with respect to the reference electrode. The electrodes were connected to the voltage follower as shown in **Figure 3A**. After a steady reading was achieved, then a precision resistor *R* was interconnected between the inputs of the voltage follower. The experiment was performed with two different precision resistors, namely 0.5 and 1.0 GΩ.. measurements.

Instrumentation: High-resolution SECM equipment supplied by Sensolytics (Bochum, Germany), was employed. The instrument was built around an Autolab (Metrohm, Herisau, Switzerland) electrochemical interface, controlled with a personal computer. Amperometric, potentiostatic and potentiometric operations were available in this configuration. For the potentiometric measurements where the Mg^{2+} sensing electrodes were employed, a voltage follower based on a 10^{13} Ω input impedance operational amplifier (TL071, Texas Instruments) was introduced in the measuring circuit [30], as shown in **Figure 4**. The cell voltage were measured with an electrometer and collected by the PC through the the electrochemical interface. The scanning system (Applicable Electronics Inc) used a 3D micro-positionar driven by precision stepping motors. The distance between the scanning tip and the substrate was usually established by allowing the probe to gently touch the sample, and subsequently the probe was generally retracted to chosen operation distance 100 µm with the aid of the *Z*-positioning motor. A video camera was used to further assist positioning of the tip close to the surface. Raster scanning was employed to record the consecutive scan lines composing the *XY* grid.

Results and Discussion

The performances of the two types of Mg^{2+} ion-selective micropipette electrodes were compared concerning their calibration, resistance, response time, and imaging stability and reproducibility when used as potentiometric tips in ISME.

For their calibration, a series of $MgCl_2$ solutions containing 1 mM NaCl as base electrolyte was employed. The range covered extended between 10^0 and 10^{-5} M Mg^{2+}. As it can be seen in **Figure 5**, both microelectrodes maintain a linear relationship at the higher concentrations. The calibration equations for the linear portions of the curves obtained for the two ISME's with the potentials were expressed in mV are:

$$E_{lc\text{-}ISME} = 87.75 - 29.12\ pMg^{2+} \quad (1)$$

$$E_{sc\text{-}ISME} = -7.47 - 33.44\ pMg^{2+} \quad (2)$$

The solid-contact microelectrode, Figure 5B attained a wider approximately linearity range to lower concentration whereas the liquid-contact electrode appeared to be insensitive to the concentration. The slopes of the linear portions (29.1 mV $decade^{-1}$ for the liquid-contact microelectrode, and interestingly 33.4 mV $decade^{-1}$ for the solid-contact one) are sufficiently close to the expected Nernstian value of 29.6 mV $decade^{-1}$ to employ these microelectrodes for quantitative measurements.

The noise present during potential measurements increases with increasing resistance of an ISME, and is therefore an indication of the expected performance of the sensors. The equivalent circuit (EC) for the resistance measurements is depicted in **Figure 5B**. Resistances of the solution and the reference electrode are also part of the system, but they are very small values compared to that of the ion-selective microelectrode. Therefore, they have not been included in the EC for the sake of simplicity. In contrast, the voltage follower has an impedance of the order of 10^{13}, ohms considerably larger than the precision resistors. Hence, once again this resistance has not been included in the EC

Figure 6 shows the current transients recorded for the liquid-contact (A) and the solid-contact (B) ISME's, respectively. After steady reading, U_R values were determined, and the resistance of the ISME was calculated using the equation describing the operation of a voltage divider:

$$R_{ISME} = R\frac{E_{OCP} - U_R}{U_R} \quad (3)$$

where E_{OCP} is the open circuit potential value established between the ISME and the external reference electrode, and U_R is the potential value measured when the resistor load R was introduced inside the electrical circuit. **Table 2** contains the resistance values obtained for micropipette electrodes of the two types. The resistance determined for the solid-contact ISME

is about a seventh of that shown by that with a liquid-contact (0.56 and 4.80 GΩ, respectively). This observation is especially relevant when considering that the size of the micropipette openings were practically the same in both cases, thus the resistance values actually arose from differences in the interfacial resistance between the internal interfaces for each system.

Another very important factor to be considered in the applicability of the Mg^{2+} ISME is their response time, which severely limits the scan rates necessary to accurately record the concentration distribution maps of a given species. This issue is especially relevant in the case of corroding systems, where the location and size of the active sites continuously vary and are followed by changes in solution concentrations due to diffusion and convection.. Ideally the scans must be recorded in a sufficiently short time to ensure that the system has not changed significantly during the measurement.

The response time of the microelectrodes was measured following the method proposed by Lamaka et al. [42] with a dual drop cell. The electrodes were immersed in one drop of 0.1 M $MgCl_2$ + 1 mM NaCl and then move to the second drop of 0.01 M $MgCl_2$ + 1 mM NaCl after a stable potential was reached in 3 minutes. The time needed to reach 95% of the total potential change caused by the change in Mg^{2+} ion concentration was regarded as response time, τ_{95}. Parameters and intervals used in the response time calculations are depicted in **Figure 7**.

Figure 8 depicts the potential changes recorded during these experiments. A visual inspection of the transients leads to the observation that the solid-contact micropipette electrode exhibits a more reproducible and stable response than the liquid-contact one. In fact, significantly shorter transient times were needed for the solid-contact ISME when quantified as τ_{95} values (namely, 71.1 s and 27.7 s were determined for the liquid-contact and the solid-contact microelectrodes, respectively). **Table 3** lists the parameters used to calculate this parameter from the dynamic response curves in Figure 8.

The performance of the two types of micropipette-based ion-selective electrodes for the imaging of Mg^{2+} ion concentration distributions was tested using the validation cell giving a source of Mg^{2+} ions 200 μm diameter pipette containing $MgCl_2$ in agar-agar. **Figure 9** gives the ISME images obtained using a liquid-contact (A), and a solid-contact (B), micropipette electrode. Both 2D ISME maps were recorded at a scan rate of 12.5 μm s^{-1}. The same pipette holding the 0.1 M $MgCl_2$ agar solution was used in the measurements plotted in Figures 9 and 10. The experiment was initiated using the solid-contact ISME The 2D array scan image in Figure 9B was recorded after about 5 to 10 minutes following immersion of the Mg^{2+} containing pipette. Subsequently, the solid-contact ISME was replaced by the liquid-contact, and array scan in Figure 9A was obtained ca. 150 minutes later. As a result of the sustained diffusion from the Mg^{2+} pipette source in the validation cell the flux of Mg^{2+} would have decreased by about 4 to 5 times according to the Cottrell equation.. Additionally, some stirring of the aqueous

solution takes place during the experiment because of unavoidable convection currents and gravitational effects due to the higher density of the $MgCl_s$ containing solution. Also the rather high scan rate employed for enhanced resolution could produce for some convective distortion. Nevertheless, the approximate circular shapes of the higher concentrations is the same as that of the pipette. Visual inspection of the two images clearly shows significant image distortion in the X-direction with the liquid-contact ISME (cf. Figure 9A) which possibly because of its slower response.

Differences in the performance of the two types of micropipette electrodes are more easily seen shown in the graphs depicted in **Figure 10**. They correspond to a sequence of scan lines taken from Figure 9 at the Y-positions indicated. It is seen that the liquid-contact microelectrode, exhibited a much boarder curve indicating a poorer electrode performance in accord with a slower response.

On the other hand, we regard these experiments with the validation cell to clearly highlight the new opportunities opened by this new solid-contact micropipette-based ion-selective electrode for the monitoring of concentration distributions of species participating in corrosion with good spatial resolution using an ISME. This hypothesis was further checked by imaging the concentration distributions of Mg^{2+} ions over a corroding magnesium sample. Separate experiments were conducted on the magnesium strip galvanically coupled to iron and at open circuit when the two metals were electrically disconnected.

Freely corroding magnesium in the chloride-containing aqueous solutions leads to the release of metal ions that were detected in ISME measurements. The concentration distributions of Mg^{2+} are shown in **Figure 11** for two separate experiments. The images of the concentrations of Mg^{2+} ions looked very different. In the case of the liquid-contact electrode, the ion concentration is rather homogeneously distributed which suggests a uniform corrosion process occurring over the entire metal strip. The morphology of the corrosive attack deduced from the inspection of Figure 11A seems to contradict the results reported in our previous work using the same type of liquid-contact ISME tip [44]. The observations derived from the analysis of a sequence of single scan lines supported the conclusion of a localized corrosive attack on the magnesium strip. The origin for such discrepancy must arise from the higher scan rates needed for recording a 2D map compared to the line scans in reference [44] which may originate blurring effects that could not be satisfactorily resolved here because of the long response times of the microelectrode. A different situation is observed when the solid-contact ISME was employed however confirms the previous result . Metal dissolution is detected from a highly localized source over the metal strip (see Figure 11B), which only covers a small fraction of the exposed metal surface. Most of the metal is thus effectively in contact with an electrolyte either free from Mg^{2+} ions or with a very low ion concentration originating from their diffusion in the electrolyte away from the actual source for the metal ions. This result is consistent with a

corroding pit or crevice corrosion located at the upper end of the magnesium strip demonstrating that he time response of the solid-contact ISME is low enough to achieve the spatial resolution required for imaging the concentration distribution of Mg^{2+} ions in the system.

Similar localized features can be observed from the inspection of the images obtained for the magnesium strip galvanically coupled to iron shown in **Figure 12**. Despite the increased number of active anodes established on the surface of the metal. with the higher concentration gradients in this system, the liquid-contact electrode also shows that the anodic activity on the metal strip occurs in a localized manner. That is, though blurring still affects the system, the high concentration met allows for better spacial resolution. than in the case of the free-corroding magnesium in Figure 11A. Indeed, very high dissolution rates for magnesium are observed when the metal was connected to iron, which are related to potential differences beyond those used for calibration of the ISME. At this stage, the negative pMg values in **Figure 12** should only be considered as semi-quantitative estimates of high local Mg^{2+} concentrations compared to lower releases over most of the metal coupon. In typical experiments, less aggressive conditions should be employed in order to detect earlier stages of the localized attack on the metal, and the linear range of the ISME calibration will thus be applicable. Despite this limitation in assessing concentration contours closely reproducing the real geometry of the reactive surface were only obtained with the solid-contact micropipette electrode despite the occurrence of hydrogen evolution.

In summary, from inspection of the ISME images in Figures 11B and 12B, the magnesium sample was observed to corrode in a heterogeneous fashion regardless the electrical condition imposed to it, as it has been previously reported [44]. The main difference imposed by galvanic coupling this metal to iron is that metal dissolution greatly increases, as evidenced by the measurement of high pMg values for the electrically-connected condition, and the observation of more than one anodic site simultaneously operating on the surface [44]. However, general corrosion was also observed to occur.

In the preceding discussion it has been assumed that the potential measured by the ISME, above the corroding magnesium surface, was solely determined by the local Mg^{2+} concentration. But it has been pointed to us [45] that there might also be an additional contribution to the measured potential difference due to the electric field present above the corroding surface. These potential differences in the electrolyte arise ohmically as a consequence of the ionic current fluxes generated by local corrosion cell, an effect that has been effectively exploited to visualize localized events in a corroding metal using the scanning reference electrode technique (SRET) [46]. Though the ISME employed in this work are not conventional micro-tip reference electrodes, they nevertheless will be subject to such effect when positioned over a corroding surface. Also SRET is influenced by the concentration of the salts of the dissolving metal as it alters the solution conductivity reducing the electric potentials.

The response of the solid-contact ISME placed over a point current source was using the Pt-Ir 100 μm dia wire microelectrode. embedded in an epoxy holder at a height of 100 μm in a solution of 1mM NaCl. Different current fluxes in the electrolyte originating from the current source were imposed. **Figure 14A** shows the current transients recorded for +564 and -662 mA cm^{-2} current densities. The ISME showed step changes in the potentials upon imposing the current that depend on the sign of the current density. Changes in potential also take place wnen the ISME was scanned over the current source as seen in **Figure 14B** which depended opn the applied current densities. In both these experiments there were variations in the background potential values. The origin of this in effect is partly related to the occurrence of water electrolysis during the experiments as evidenced by observation of vigorous gas evolution as recorded through the video camera. This reaction produces major local pH changes at both electrodes, which effectively affect the offset potential value of the ISME because the ionophore exhibits a Nernstian response towards protons activity in acidic solution [43] and there was no Mg^{2+} ions in the electrolyte to buffer the potential allowing the potential to float. The relevance of the pH changes during the measurements was imaged with the video camera when a pH indicator (namely phenolphthalein) was added to the electrolyte immediately after removal of the ISME from the solution (see **Figure 15**). Therefore, the slow potential variations seen in Figures 14A and 14B using a Pt-Ir microelectrode as current source could not be unambiguously related to the effect of a potential field in the electrolyte as they were influenced by the unavoidable changes produced during the measurements at the interface of the ionophore and the bulk electrolyte. The bubbles produced by the electrolysis may also have contributed to other errors. In **Figure 14B** the full width at half height of 1300 μm was much larger than expected and may be a result of bubbles adhering to the scanning tip of the electrode which has been observed. Nevertheless, in contrast to these uncertainties the important observation in Figure 14A is the immediate step change following application or removal of the current flow. These changes occurred too rapidly to be a result of interfacial effects which were seen to be slow. The variations in potential in **Figure 14B**

In order to overcome the problems originated by the use of a noble metal disk electrode as current point source, a new

We attempted to measure the response of the solid-contact ISME over 100 μm diameter Pt-Ir current source embedded in an epoxy holder. However, the measurements were poor and attributable to the changes in pH and bubbles that formed on the surface due to water electrolysis during the experiment observation of vigorous gas evolution. The presence of bubbles and pH changes during these measurements was confirmed by video camera imaging when a pH indicator, phenolphthalein, was added to the electrolyte. The indicator changes from colorless to purple at the concentrations used. The purple coloration is seen at the cathodes and a corresponding acidic formation occurs at the anode. The pH changes affect the offset

potential of the ISME because the ionophore exhibits a Nernstian response towards protons activity in acidic solution [43]. The bubbles adhering to the electrodes also tended to adhere to the tip of the ISME and they distorted the current flow directions.

Using a glass micropipette overcame the pH and the bubbles effects a The solid-contact ISME placed 140 μm from its tip. In **Figure 15** it can be seen that the background potential of the ISME remains virtually constant throughout all the measurements as indicated by the drawn dotted lines. The application of different current densities ranging from 4.5 to 28.5 mA cm^{-2} produce potential changes in the ISME amounting 3-18 mV, respectively. Scan lines are shown in Figure 16B. The scans produced well defined potential peaks without perfectly symmetry. This feature is attributed to the practical difficulties found in order to produce perfectly symmetrical glass capillary openings parallel to the scan direction. Despite these practical limitations, the potential changes occurring at the ISME clearly reflect the magnitude and the sign of the electric field developed from the glass micropipette current source. Next, a stable potential response of the ISME was found at the end of the experiment when it was scanned over the glass micropipette current source whereas no current was flowing in the cell. ???An important observation in **Figure 15A** is the rapid change following application or removal of the current flow. The changes, particularly those on disconnecting the current, occurred too rapidly to be a result of interfacial effects. Delays in the response were less than about 20s which were seen with the larger cathodic currents.

The magnitude of the potential change originated by the variation of the electric field in the electrolyte can be determined from the potential transients given in Figure 16A. Very interestingly, a linear relationship was established between these two parameters, thus allowing the response of the ISME to be calibrated regarding an electric field operating in the solution where the concentration of the ion being monitored does not change. Current densities in excess of 30 mA cm^{-2} must be flow from a current source located 140 μm from the probe to produce a potential change of 20 mV, which would be equivalent to a change in the magnesium concentration smaller than one order of magnitude. Furthermore, the effect of the electric field can be regarded to be negligible if the current flowing in the cell is 10 times smaller, values typically operating in the case of a Fe-Mg galvanic couple as the one described in our work.

Conclusion

A new ISME construction to investigate corrosion processes on magnesium-based or magnesium-containing materials with high spatial resolution has been presented. It is based on a robust solid-contact with the ionophore which exhibits smaller internal resistance and a faster

response times compared to one with a conventional liquid-contact having the same tip dimensions. Both types of magnesium ion measuring micropipette probes were successfully employed to perform *in situ* experiments on model corroding systems. The solid-contact ISME with its greater stability and lower internal impedance had a marked impact on the ability to collect these images with a high spatial resolution needed to study early stages of localized corrosion. Most of the corrosion studies were due to localized pitting and crevice corrosion but examples of general corrosion were seen. In the corrosion experiments the observed potential changes with the ISME were possibly attributed to both changes in Mg^{2+} concentrations and to corrosion currents. The Nernstian potential changes due to the Mg^{2+} concentrations were much larger than the those produced by the ohmic electric potentials in solution.

Acknowledgments

The authors are grateful to the Spanish Ministry of Science and Innovation (MICINN, Madrid, Acción Integrada No. HH2008-0011) and to the National Office for Research and Technology (NKTH, Budapest, research grant ES-25/2008 TeT) for the grant of a Collaborative Research Programme between Hungary and Spain. J.J.S., J.I. and R.M.S. are grateful for financial support by the MICINN and the European Regional Development Fund (Brussels, Belgium) under Projects No. CTQ2009-12459 and CTQ2012-36787. A Research Training Grant awarded to J.I. by the Spanish Ministry of Education (MECD, Madrid, *Programa de Formación de Personal Investigador*) is gratefully acknowledged. A.K., L.N., and G.N. acknowledge support from "Developing Competitiveness of Universities in the South Transdanubian Region (SROP-4.2.1.B-10/2/KONV-2010-0002)".H.S.I. acknowledges work supported by U.S. Department of Energy, Divisions of Chemical and Material Sciences, under the Contract No. DE-AC02-98CH10886 and the University of La Laguna for supporting his scientific visit to Tenerife (Spain).

References

1. M.M. Avedesian, in *ASM Handbook*, *Vol. 13, Corrosion,* ASM International, 4th Edition, Metals Park, OH, **1992**.
2. D. Eliezer, E. Aghion, and F.H. Froes, *Adv. Performance Mater.* **5**, 201 (1998).
3. G.L. Song and A. Atrens, *Adv. Eng. Mater.*, **1**, 11 (1999).
4. R.C. Zeng, J. Chen, W. Dietzel, R. Zettler, J.F. Dos Santos, M. Lucia Nascimento, and K.U. Kainer, *Corros. Sci.*, **51**, 1738 (2009).

5. G. Song, A. Atrens, D. St John, J. Nairn, and Y. Li, *Corros. Sci.*, **39**, 855 (1997).
6. G.L. Song, A. Atrens, X.L. Wu, and B. Zhang, *Corros. Sci.*, 40, 1769 (1998).
7. R. Ambat, N.N. Aung, and W. Zhou, *Corros. Sci.*, **42**, 1433 (2000).
8. S. Bender, J. Goellner, A. Heyn, and E. Boese, *Mater. Corros*., **58**, 977 (2007).
9. T.R. Thomaz, C.R. Weber, T. Pelegrini, L.F.P. Dick, and G. Knörnschild, *Corros. Sci.*, **52**, 2235 (2010).
10. N.T. Kirkland, G. Williams, and N. Birbilis, *Corros. Sci.*, **65**, 5 (2012).
11. W.A. Ferrando, *J. Mater. Eng.*, **11**, 299 (1989).
12. A.-M. Lafront, W. Zhang, S. Jin, R. Tremblay, D. Dubé, and E. Ghali, *Electrochim. Acta*, 51, 489 (2005).
13. M.C. Zhao, M. Liu, G.L. Song, and A. Atrens, *Corros. Sci.*, **50**, 3168 (2008).
14. G.L. Song and Z. Xu, *Electrochim. Acta*, **55**, 4148 (2010).
15. Z. Szklarska-Smialowska*, Corros. Sci.*, **41**, 1743 (1999).
16. G. Song and A. Atrens, *Adv. Eng. Mater.*, **9**, 177 (2007).
17. P. Brouillet, I. Epelboin, and M. Froment, *C.R. Acad. Sci.,* **239**, 1795 (1954).
18. R.L. Petty, A.W. Davidson, and J. Kleinberg, *J. Amer. Chem. Soc.*, **76**, 363 (1954).
19. A. Atrens and W. Dietzel, *Adv. Eng. Mater.*, **9**, 292 (2007).
20. D. Sadcheva, *Corros. Sci.*, **60**, 18 (2012).
21. G.L. Song, A. Atrens, and D. StJohn, in *Magnesium Technology 2001*, pp. 255-262, TMS, New Orleans, LA (2001).
22. G. Baril, G. Galicia, C. Deslouis, N. Pébère, B. Tribollet, V. Vivier, *J. Electrochem. Soc.*, **154**, C108 (2007).
23. G. Williams and H.N. McMurray, *J. Electrochem. Soc.*, **155**, C340 (2008).
24. J. Światowska, P. Volovitch, and K. Ogle, *Corros. Sci.*, **52**, 2372 (2010).
25. G. Williams and R. Grace, *Electrochim. Acta*, **56**, 1894 (2011).
26. S.E. Pust, W. Maier, G. Wittstock, *Z. Phys. Chem. (Muenchen Ger.)*, 222, 1463 (2008).
27. L. Niu, Y. Yin, W. Guo, M. Lu, R. Qin, and S. Chen, *J. Mater. Sci.*, **44**, 4511 (2009).
28. M.B. Jensen and D.E. Tallman, in *Electroanalytical Chemistry: A Series of Advances,* Vol. 24, A.J. Bard and C.G. Zoski, Editors, pp. 171-286, CRC Press, Boca Raton, FL (2012).
29. R.M. Souto, Y. González-García, D. Battistel, and S. Daniele, *Chem. Eur. J.*, **18**, 230 (2012).
30. R.M. Souto, J. Izquierdo, J.J. Santana, A. Kiss, L. Nagy, and G. Nagy, in *Current Microscopy Contributions to Advances in Sciences and Technology,* Vol. 2, A. Méndez-Vilas, Editor, pp. 1407-1415, Formatex Research Center, Badajoz, Spain (2012).
31. G. Gyetvai, S. Sundblom, L. Nagy, A. Ivaska, and G. Nagy, *Electroanalysis*, **19**, 1116 (2007).
32. G. Gyetvai, L. Nagy, A. Ivaska, I. Hernádi, and G. Nagy, *Electroanalysis*, **21**, 1970 (2007).

33. J. Izquierdo, L. Nagy, Á. Varga, I. Bitter, G. Nagy, and R.M. Souto, *Electrochim. Acta*, **59**, 398 (2012).
34. J. Izquierdo, L. Nagy, J.J. Santana, G. Nagy, and R.M. Souto, *Electrochim. Acta*, **58**, 707 (2011).
35. B. Czoka, and Z. Mekhalif, *Electrochim. Acta*, **54**, 3225 (2009).
36. J. Izquierdo, L. Nagy, J.J. Santana, R.M. Souto, and G. Nagy, *Electrochim. Acta*, **56**, 8846 (2011).
37. B. Horrocks, M.V. Mirkin, D.T. Pierce, A.J. Bard, G. Nagy, and K. Toth, *Anal. Chem*., **65**, 1213 (1993).
38. M.V. Rouilly, M. Badertscher, E. Pretsch, G. Suter, and W. Simon, *Anal. Chem.*, **60**, 2013 (1988).
39. U.E. Spichiger, R. Eugstrer, E. Haase, G. Rumpf, P.M. Gehrig, A. Schmid, B. Rusterholz, and W. Simon, *Fresenius J. Anal. Chem.*, **341**, 727 (1991).
40. Z. Hu and D. Qi, *Anal. Chim. Acta*, **248**, 177 (1991).
41. S.V. Lamaka, O.V. Karavai, A.C. Bastos, M.L. Zheludkevich, and M.G.S. Ferreira, *Electrochem. Commun.*, **10**, 259 (2008).
42. S.V. Lamaka, M.G. Taryba, M.L. Zheludkevich, and M.G.S. Ferreira, *Electroanalysis*, **21**, 2447 (2009).
43. K. Tóth, E. Lindner, M. Horváth, J. Jeney, E. Pungor, I. Bitter, B. Ágai, and L. Töke, *Electroanalysis*, **5**, 781 (1993).
44. J. Izquierdo, L. Nagy, I. Bitter, R.M. Souto, and G. Nagy, *Electrochim. Acta*, **87**, 283 (2013).
45. Comment raised by a reviewer to the manuscript. Authors are greatly indebted for his valuable contribution.
46. H.S. Isaacs and B. Vyas, in *Electrochemical Corrosion Testing*, F. Mansfeld and U. Bertocci, Editors, pp. 3-33, ASTM, Baltimore, MD (1981).

Table 1. Composition of the mixture employed to produce the cocktail for the Mg^{2+} ion-selective microelectrodes.

Component	Quantities for 200 µl of the mixture	
	Content	wt.%
Tetrahydrofurane (THF)	100 µL	-
Poly(vinyl chloride) (PVC)	7.68 mg	5.06
bis-N,N-dicyclohexyl-malonamide	2.23 mg	1.47
Potassium tetrakis(4-chlorophenyl)borate (PTCB)	2.13 mg	1.40
2-nitrophenyl octyl ether (oNPOE)	139.79 mg	92.07

Table 2. Resistance measurements for the two kinds of Mg^{2+} ion-selective micropipette electrodes conducted in 1 mM $MgCl_2$ + 1 mM NaCl solution.

Parameter	ISME	
	Liquid-contact	Solid-contact
E_{OCP}, mV	-49.5	-75.7
R, GΩ	1	1
U_R, mV	-8.53	-48.41
R_{ISME}, GΩ	**4.80**	**0.56**

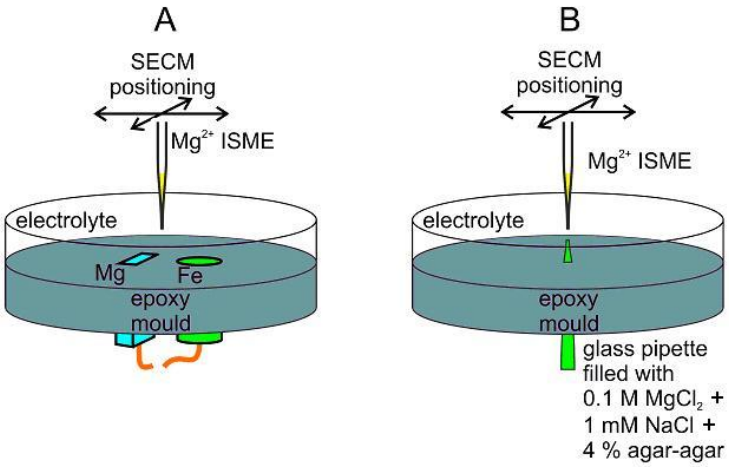

Figure 1. Sketches of the electrochemical cells employed: (A) galvanic Fe-Mg system; (B) validation cell supporting a glass pipette filled with $MgCl_2$ solution.

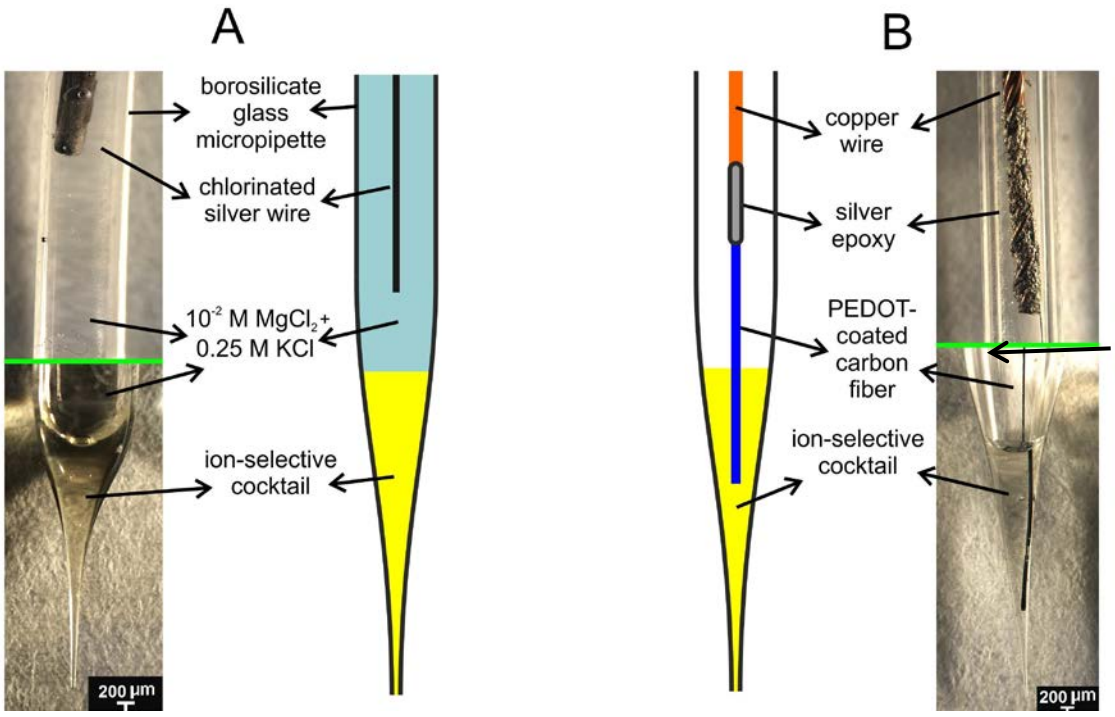

Figure 2. Sketches and micrographs of the micropipette electrodes fabricated for the selective detection of Mg^{2+} ions: (A) liquid-contact, and (B) solid-contact ISME's.

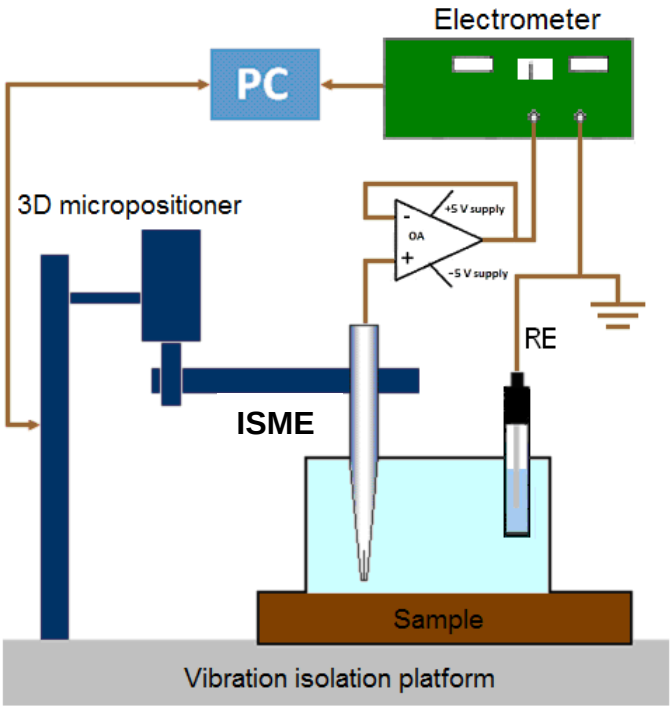

Figure 3. Sketch showing the main components of the instrument employed, including the high input impedance operational amplifier (OA), and the ion-selective electrode (ISME).

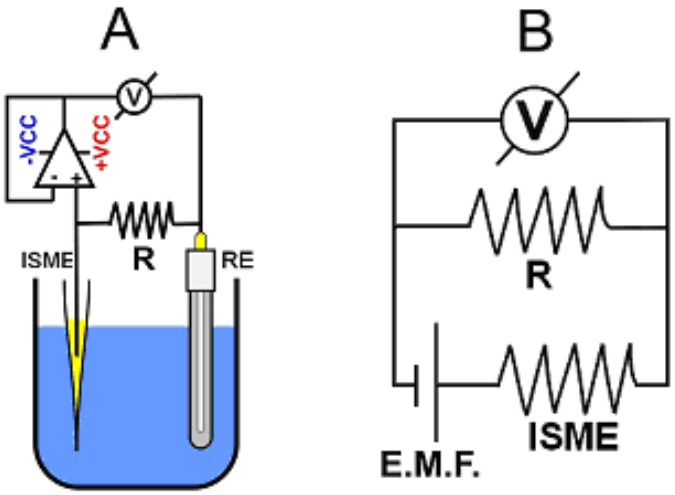

Figure 4. (A) Sketch of the electrochemical cell used for the measurement of the internal resistance of the ISME, and (B) equivalent circuit.

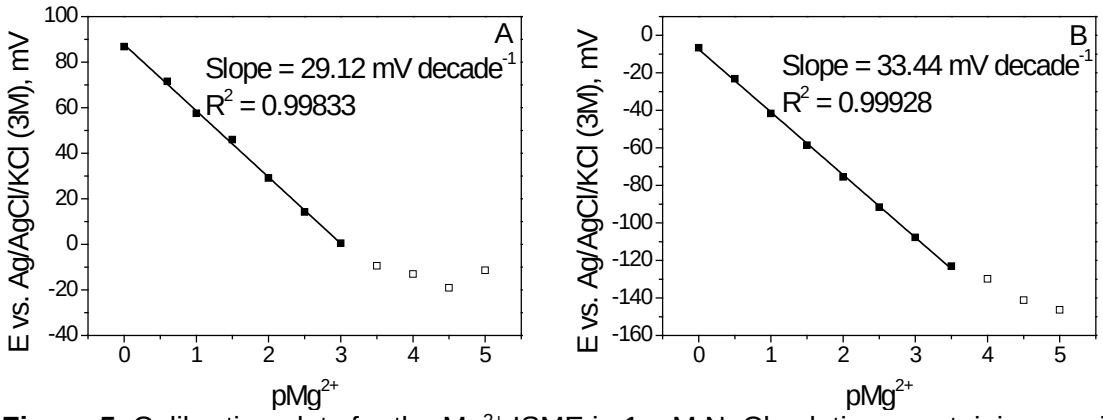

Figure 5. Calibration plots for the Mg^{2+} ISME in 1 mM NaCl solutions containing varying amounts of $MgCl_2$ ($pMg = -\log_{10}[Mg^{2+}]$). (A) Liquid-contact, and (B) solid-contact

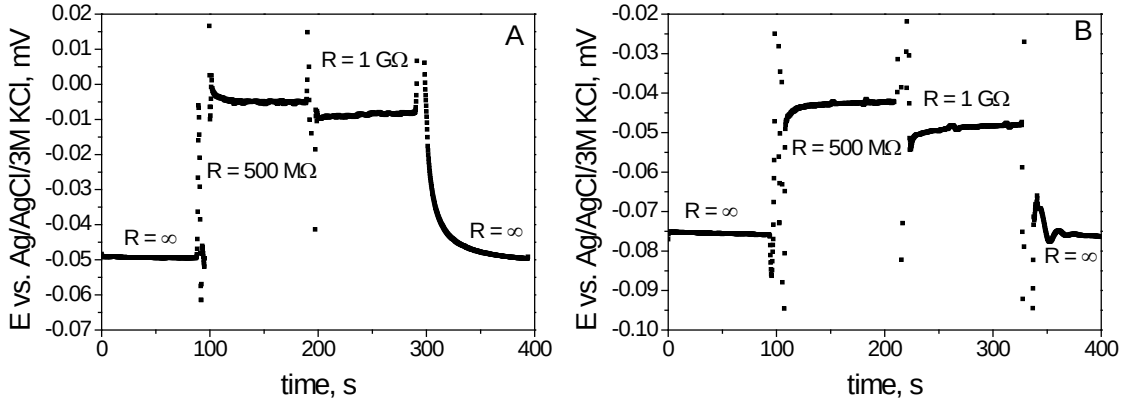

Figure 6. Response of ISME to shorting resistors for the voltage divider method: (A) Liquid-contact, and (B) solid-contact.

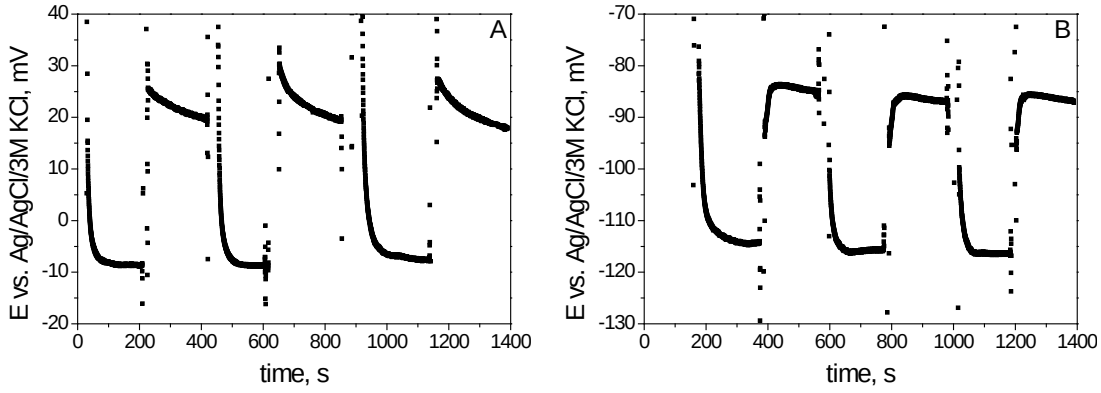

Figure 7. Dynamic response curves obtained for response time measurements to changes in $MgCl_2$ concentrations between 10^{-1} M and 10^{-2} M, in 10^{-3} M NaCl. (A) liquid-contact, and (B) solid-contact Mg^{2+} ISME.

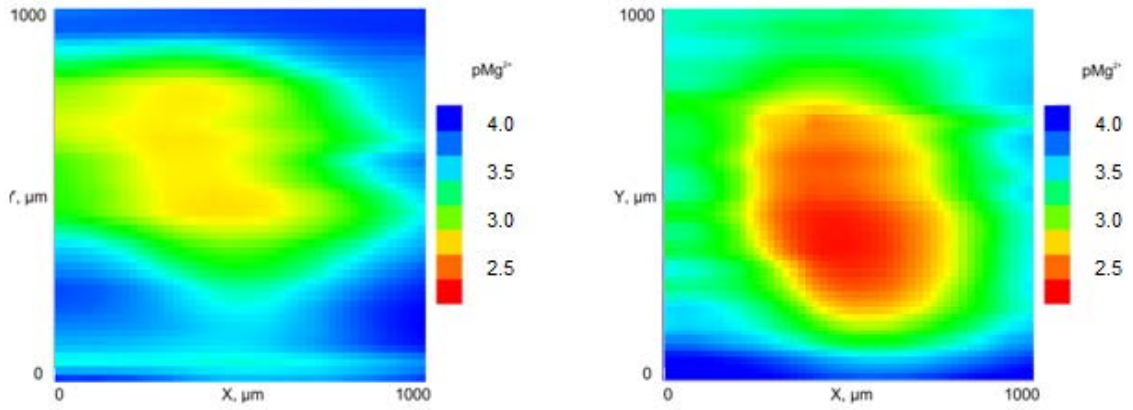

Figure 8. ISME images displaying the of Mg^{2+} ion concentrations 100 µm; above the tip of a centered pipette source (A) liquid-contact, and (B) solid-contact. Scan rate: 12.5 µm s^{-1}.

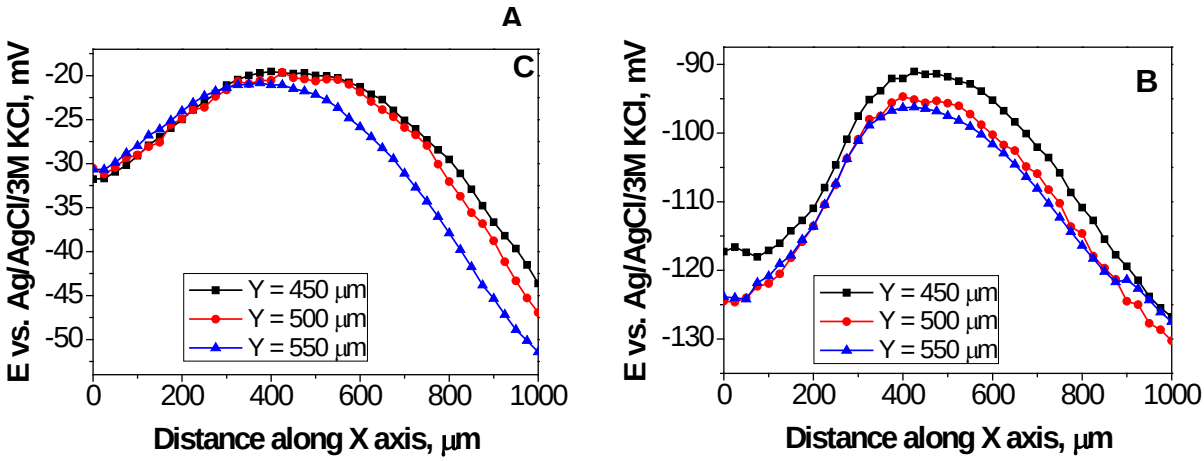

Figure 9. (Color online) Line scans displaying the distribution of Mg^{2+} ion concentration close to the centre of the magnesium ion pipette source. (A) liquid-contact, and (B) solid-contact ISME's. The scans were extracted from the middle of the SECM images given in Figure 8. Tip-substrate distance: 100 µm; scan rate: 12.5 µm s^{-1}.

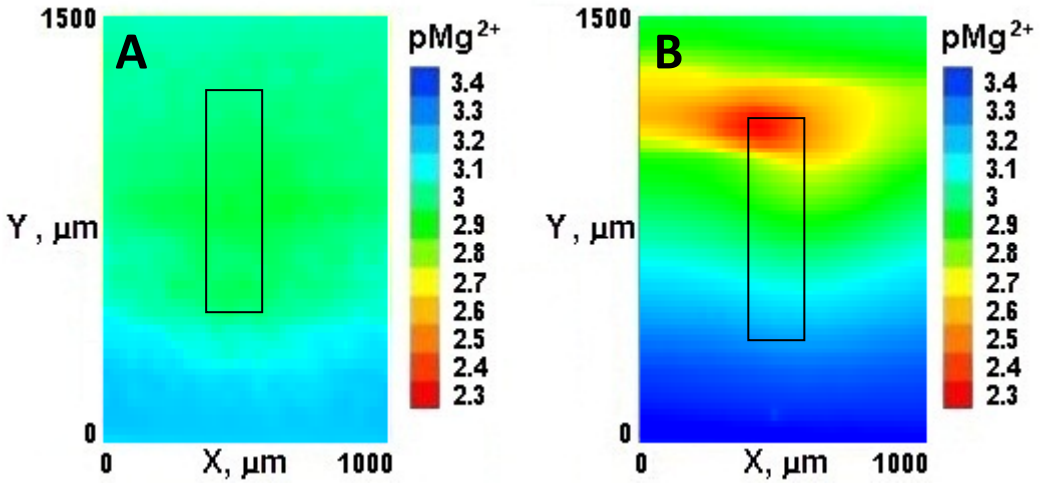

Figure 10. Mg^{2+} ion concentration images above freely corroding magnesium in 10 mM NaCl. (A) liquid-contact, and (B) solid-contact. Tip-substrate distance: 100 µm; scan rate: 12.5 µm s^{-1}. The location of the magnesium strip is drawn on the images.

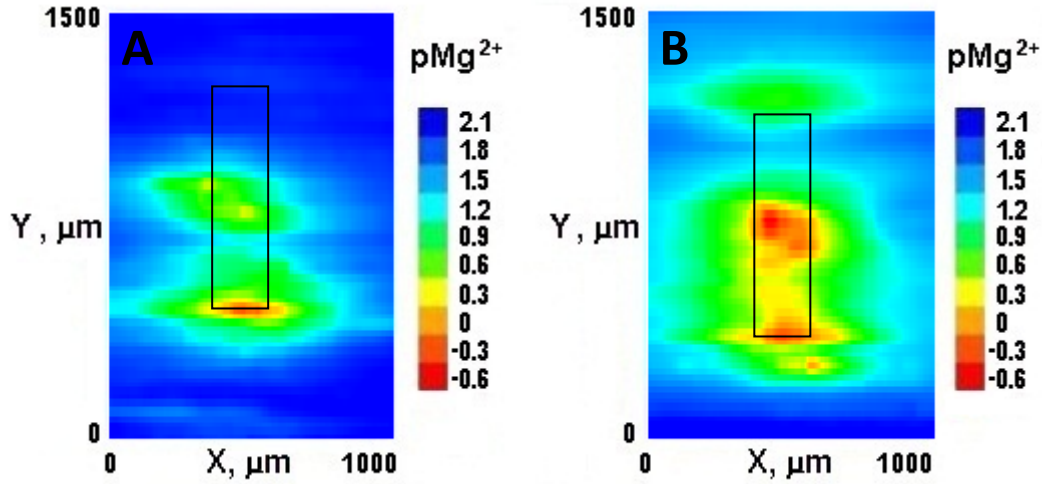

Figure 11. Mg^{2+} ion concentration images above a magnesium strip galvanically shorted to iron in 10 mM NaCl solution (A) liquid-contact, and (B) solid-contact. The position of the iron strip was 5 mm to the right of the magnesium strip in the images. Tip-substrate distance: 100 µm; scan rate: 12.5 µm s^{-1}.

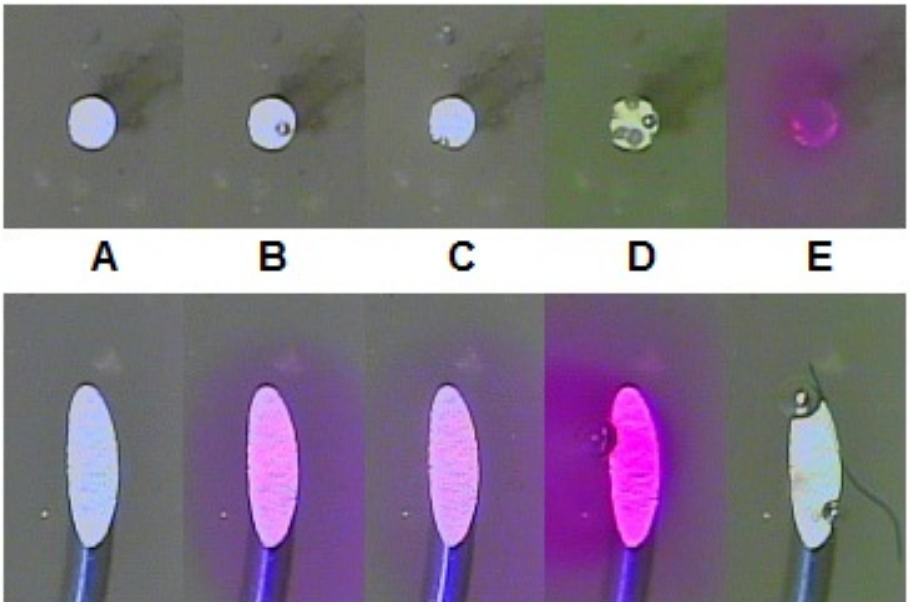

Figure 12. pH response around Pt-Ir electrodes in 1 mM NaCl solution containing phenolphtalein indicator: (A) electrodes disconnected and carrying density currents of: (B) 38.5, (C) 54.6, (D) 550, and (E) -645 mA cm^{-2} flowing in solution from the disc to the ellipse electrode.

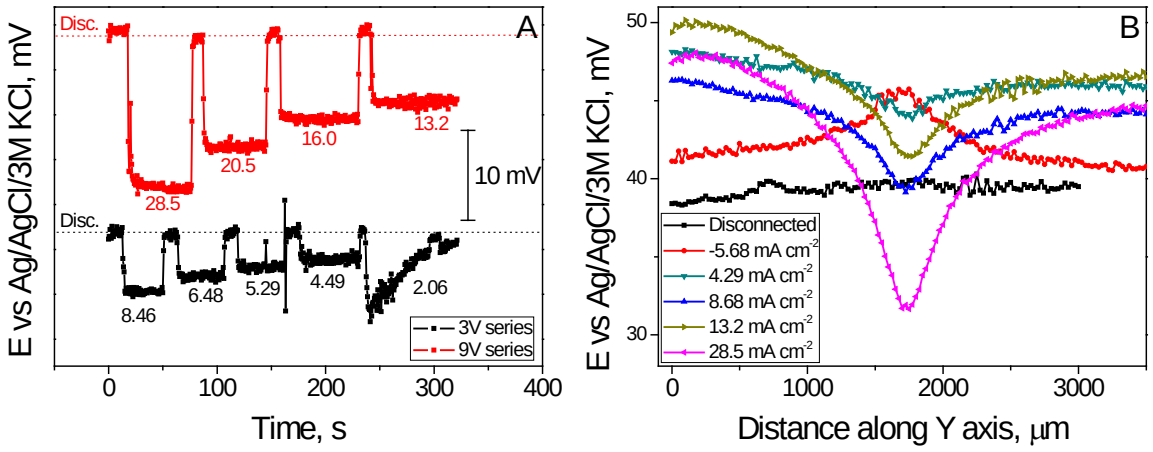

Figure 13. Potential response of a solid-contact Mg^{2+} ISME in 1 mM NaCl solution to currents from a glass micropipette current source. (A) Probe distance: 100 μm.; (B) line scans over the source. The center of the line was 100 μm above source ; scan rate: 12.5 μm s^{-1}. The values of the current densities indicated in (A) are given in mA cm^{-2}.

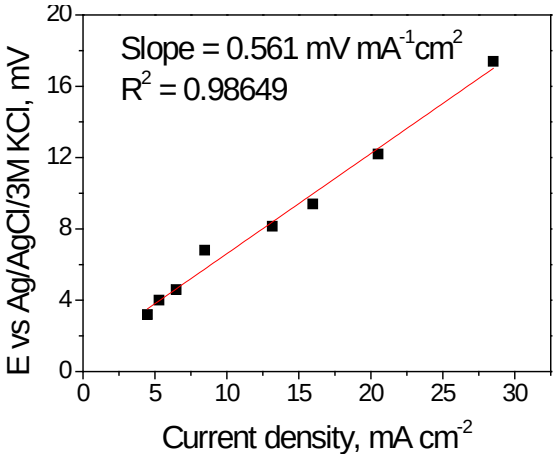

Figure 14. Calibration plot for the potential response of the solid-contact Mg^{2+} ion selective micropipette electrode with the amount of current flowing in the solution from a glass micropipette current source. The ISME was 100 µm above the glass micropipette current source.